

# Electrocatalytic Activity of Palladium Nanocatalysts Supported on Carbon Nanoparticles in Formic Acid Oxidation

Jie Huang<sup>1,2</sup>, Zhiyou Zhou<sup>1</sup>, Yang Song<sup>1</sup>, Xiongwu Kang<sup>1</sup>, Ke Liu<sup>1</sup>,  
Wancheng Zhou<sup>2</sup>, Shaowei Chen<sup>1\*</sup>

(1. Department of Chemistry and Biochemistry, University of California, Santa Cruz, California 95064, United States; 2. State Key Laboratory of Solidification Processing, Northwestern Polytechnical University, Xi'an 710072, China)

**Abstract:** Palladium nanostructures were deposited onto carbon nanoparticle surface by a chemical reduction method. Transmission electron microscopic studies showed that whereas the resulting metal-carbon (Pd-CNP) nanocomposites exhibited a diameter of 20 to 30 nm, the metal components actually showed a cauliflower-like surface morphology that consisted of numerous smaller Pd nanoparticles (3 to 8 nm). Electrochemical studies showed that the effective surface area of the Pd-CNP nanoparticles was about 40% less than that of Pd black, possibly because the Pd nanoparticles were coated with a layer of carbon nanoparticles; yet, the Pd-CNP nanocomposites exhibited marked enhancement of the electrocatalytic activity in formic acid oxidation, as compared to that of Pd black. In fact, the mass- and surface-specific activities of the former were about three times higher than those of the latter. This improvement was likely a result of the enhanced accessibility of the Pd catalyst surface and the formation of abundant active sites of Pd on the carbon nanoparticle surface due to the hierarchical structure of the metal nanocatalysts.

**Key words:** palladium nanostructure; carbon nanoparticle; formic acid oxidation; fuel cell

**CLC Number:** TM911.4

**Document Code:** A

## 1 Introduction

Fuel cells are of tremendous interest because of their high energy conversion efficiency and low environmental pollution. Up to now, one of the major problems in small molecule (e.g., methanol or formic acid) fuel cells is the poisoning of the electrocatalysts by CO formed during the incomplete oxidation of the organic fuels<sup>[1]</sup>. In comparison with methanol, formic acid (HCOOH) has several unique advantages, such as fast oxidation kinetics, low toxicity and low crossover rate through the Nafion membrane. Therefore, direct formic acid fuel cells (DFAFCs) have been hailed as a

promising power source for portable electronic devices and automobiles, and have attracted considerable interest in recent years<sup>[2-3]</sup>. However, the commercialization of DFAFCs is largely impeded by the poor performance of anodic catalysts for HCOOH electrooxidation. So far, two types of catalysts, Pd- and Pt-based nanoparticles, have often been used for HCOOH electrooxidation. Of these, Pt catalysts typically exhibit a high intrinsic activity. But they are vulnerable to surface poisoning by adsorbed CO (CO<sub>ad</sub>), a reaction intermediate<sup>[4]</sup>. In contrast, Pd is free of CO<sub>ad</sub> poisoning in the short term, and

Received: 2012-01-20, Revised: 2012-02-01 \*Corresponding author, Tel: +1 (831) 459-5841, E-mail: shaowei@ucsc.edu

This work was supported, in part, by the National Science Foundation (CHE-1012256 and DMR-0804049) and by the ACS-Petroleum Research Fund (49137-ND10). J. Huang was supported, in part, by a research fellowship from the China Scholarship Council. TEM work was performed as a User Project at the National Center for Electron Microscopy, Lawrence Berkeley National Laboratory, which is supported by the US Department of Energy.

formic acid is mainly oxidized via the direct pathway<sup>[5-6]</sup>. To further improve the catalytic activity, especially the activity per mass of precious metals, several strategies have been employed that typically involve rational control of the chemical composition, size and surface structures (such as crystalline planes and surface ligands) of the nanoparticle catalysts<sup>[7-9]</sup>. In addition, recently we have shown that the performance of Pd and Pt nanoparticle catalysts in formic acid oxidation could be significantly improved in acidic media by deliberate chemical functionalization with organic capping ligands<sup>[10-11]</sup>. However, as both Pt and Pd are costly and the reserves are limited, high loading of expensive Pd or Pt on carbon has impeded their use in fuel cells. Therefore, there is an urgent need to develop electrocatalysts with low Pd loadings.

Typically, nanoparticle catalysts are dispersed on high surface area carbons, such as carbon nanotubes, carbon black, and activated carbon fibers, so as to enhance accessibility of the nanoparticle surface as well as to stabilize and even to enhance the electrocatalytic performance<sup>[12]</sup>. In contrast, reports of the applications of nanometer-sized carbon particles as electrocatalyst support have been scarce. Note that carbon nanoparticles (CNPs) represent a unique, and relatively new, class of functional carbonaceous materials that warrant further and more thorough investigation. For instance, we recently demonstrated that fluorescent CNPs (dia.  $4.8 \pm 0.6$  nm) could be readily prepared by thermal refluxing of natural gas soot in concentrated nitric acid and selected metal (e.g., Pd, Ag, Cu, etc.) nanostructures might be deposited onto the resulting nanoparticle surface<sup>[13]</sup>. In this paper, we carried out a detailed electrochemical study to examine the electrocatalytic activity of the CNP-supported Pd nanostructures in formic acid oxidation. The results were much better than those of commercial Pd black. Additionally, the steady-state

mass current density was markedly improved.

## 2 Experimental

### 2.1 Chemicals

Nitric acid (HNO<sub>3</sub>, 69.8%, Fisher), sulfuric acid (H<sub>2</sub>SO<sub>4</sub>, 98%, Fisher), formic acid (HCOOH, 99%, ACROS), sodium carbonate (Na<sub>2</sub>CO<sub>3</sub>, 99%, Aldrich), palladium chloride (PdCl<sub>2</sub>, MP Biomedicals), and ascorbic acid (99%, ACROS) were all used as received. Water was supplied by a Barnstead Nanopure Water System (18.3 MΩ·cm).

### 2.2 Synthesis of Carbon Nanoparticles

The procedure has been described previously<sup>[13-15]</sup>. Briefly, carbon soot was collected on the inside wall of a glass beaker by placing the beaker upside-down above the flame of a natural gas burner. Typically 100 mg of the soot was then refluxed in 10 mL of 5 mol·L<sup>-1</sup> HNO<sub>3</sub> for 12 h. When cooled down to room temperature, the brownish yellow supernatant after centrifugation was neutralized by Na<sub>2</sub>CO<sub>3</sub> and then dialyzed against Nanopure water through a dialysis membrane for 3 days, affording purified CNPs which exhibited an average core diameter of  $(4.8 \pm 0.6)$  nm with well-defined graphitic crystalline lattices, as determined by high-resolution transmission electron microscopic measurements<sup>[13-15]</sup>.

### 2.3 Carbon-Supported Palladium Nanoparticles

Carbon-supported Pd nanoparticles were synthesized by mixing PdCl<sub>2</sub>, ascorbic acid, and CNPs in water, as described previously<sup>[13]</sup>. In a typical experiment, 10 mg of CNPs was dissolved in 10 mL of water. Then 1 mL of a PdCl<sub>2</sub> solution at a concentration of 1 mg·mL<sup>-1</sup> in water was added into the carbon particle solution under magnetic stirring. The mixture was allowed to stir overnight, to which a calculated amount of ascorbic acid was added in a slow dropwise fashion. The solution color changed gradually from light brown to dark brown, signifying the formation of Pd nanostructures. Excessive

salts were then removed by dialysis against Nanopure water, and the carbon-supported palladium nanoparticles (denoted as Pd-CNP) remained soluble in water.

## 2.4 Transmission Electron Microscopy (TEM)

The particle core diameter and lattice fringes were examined with a JEOL 2100-F200 kV Field-Emission Analytical Transmission Electron Microscope in the National Center for Electron Microscopy at Lawrence Berkeley National Laboratory. The samples were prepared by casting a drop of the particle solution ( $\sim 1 \text{ mg} \cdot \text{mL}^{-1}$ ) in Nanopure water onto a 200-mesh holey carbon-coated copper grid. The particle diameter was estimated by using ImageJ<sup>®</sup> software analysis of the TEM micrographs.

## 2.5 Electrochemistry

Cyclic voltametric measurements were carried out with a CHI 440 electrochemical workstation. A glassy carbon electrode (GC,  $\Phi = 5 \text{ mm}$ , from Bioanalytical Systems, Inc.) was used as the working electrode. A saturated calomel electrode (SCE) and a Pt coil were used as the reference and counter electrodes, respectively. The GC was first polished with  $0.03 \mu\text{m}$  alumina slurries and then cleansed by sonication in Nanopure water. The electrolyte solutions were deaerated with ultrahigh purity  $\text{N}_2$  for 10 min before the acquisition of electrochemical data, and the electrolyte solution was blanketed with a nitrogen atmosphere during the entire experimental procedure.

## 3 Results and Discussion

As mentioned above, the Pd-CNP nanoparticles were prepared by mixing  $\text{PdCl}_2$  and ascorbic acid with CNPs in water. The ascorbic acid served as a reducing agent, where the reduction of Pd metal ions and the generation of Pd particles were presumably facilitated by the complex formation between Pd ions and CNPs through the peripheral carboxylic moieties<sup>[13]</sup>. The morphological details of the Pd-CNP

nanoparticles were first characterized by TEM measurements. Fig. 1A shows a representative bright-field TEM micrograph of the Pd-CNP nanoparticles. It can be seen that the particles are mostly of spherical shape and dispersed rather evenly on the TEM grid, with the majority of the particles in the range of 20 to 30 nm in diameter. Note that the average diameter of individual CNPs is less than 5 nm<sup>[13]</sup>. Additionally, a light-contrast halo ring can be seen wrapping around the dark-contrast metal nanostructure, suggesting that the metal nanostructures were actually stabilized by a carbon overlayer that rendered the particles soluble in water, as observed earlier<sup>[13]</sup>.

More structural insights of the Pd-CNP nanoparticles can be obtained in dark-field TEM studies, as exemplified in Fig. 1B. One can see that the Pd-CNP nanoparticles were actually composed of a large number of nanometer-sized Pd particles (3 to 8 nm), with a surface morphology analogous to that of a cauliflower. High-resolution TEM (HRTEM) images indeed show well-defined crystalline lattice fringes that are most likely attributable to metallic Pd. Fig. 1C depicts a representative HRTEM micrograph where a lattice spacing of 0.237 nm can be clearly identified (white lines and arrows). This is markedly different from that expected for the spacing between the  $\{111\}$  lattice planes (0.2246 nm) of face-centered cubic (fcc) Pd. Instead, it is rather consistent with the fringe spacing (0.2382 nm) of the kinematically forbidden  $1/3\{422\}$  reflections that have been observed in palladium thin films or platelets with  $\{111\}$  surfaces and rather small thicknesses in the perpendicular direction<sup>[16-18]</sup>.

The distribution of the metal components within the nanoparticles was further analyzed by high-resolution elemental mapping. Fig. 1D shows the line scans of the Pd and C elements within the Pd-CNP nanoparticles. Overall, both elements

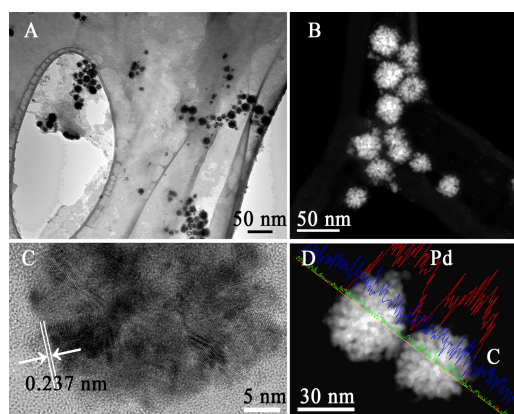


Fig. 1 Representative bright-field (A) and dark-field (B) transmission electron micrographs of Pd-CNP nanoparticles. Panel (C) depicts the high-resolution image of a Pd-CNP nanoparticle, and Panel (D) shows the elemental mapping of a pair of Pd nanoparticles where the upper curve represents the distribution of Pd and the middle curve for C.

appeared to be distributed rather homogeneously across the entire Pd-CNP nanoparticles, although the spikes seemed to suggest a hierarchical architecture within the nanoparticles, as shown in Fig. 1B.

The electrocatalytic activity of these Pd-CNP nanoparticles in formic acid oxidation was then examined by electrochemical measurements. Fig. 2 shows the cyclic voltammograms of a GC electrode modified with the Pd-CNP nanoparticles (solid curve) and Pd black (dashed curve) in  $0.1 \text{ mol} \cdot \text{L}^{-1} \text{ H}_2\text{SO}_4$  at a potential sweep rate of  $0.1 \text{ V} \cdot \text{s}^{-1}$ . The currents have been normalized to the respective mass loading of Pd. The voltammetric feature between  $-0.25 \text{ V}$  and  $0.0 \text{ V}$  can be ascribed to the adsorption/desorption of hydrogen and (bi)sulfate on the Pd surfaces, as well as absorption of a small fraction of hydrogen into the Pd metal lattice<sup>[19-21]</sup>. A well-defined cathodic peak at around  $0.35 \text{ V}$  can be observed which is assigned to the reduction of Pd oxide that was formed in the positive potential scan. Woods et al.<sup>[22]</sup> have reported that a monolayer of Pd oxide would be formed on the Pd surface at  $1.5 \text{ V}$

(vs. RHE), which is equivalent to ca.  $1.20 \text{ V}$  (vs. SCE) in  $0.1 \text{ mol} \cdot \text{L}^{-1} \text{ H}_2\text{SO}_4$  in the present study, and the reduction of the Pd oxide corresponds to a charge density of  $424 \mu\text{C} \cdot \text{cm}^{-2}$ . This provides a convenient method to determine the electrochemical surface area (ECSA) of Pd, without the complication of surface contamination, as observed with other methods<sup>[7, 23]</sup>. From Fig. 2, the ECSA of the Pd-CNP modified electrode was estimated to be  $12.3 \text{ m}^2 \cdot \text{g}^{-1}$ , about 40% smaller than that of commercial Pd black ( $17.2 \text{ m}^2 \cdot \text{g}^{-1}$ ), primarily because of the coating of the Pd surfaces by carbon (Fig. 1).

Nevertheless, the Pd-CNP nanoparticles exhibited much enhanced electrocatalytic activity in formic acid oxidation. Fig. 3 depicts the cyclic voltammograms of the Pd-CNPs and Pd black recorded in a  $0.1 \text{ mol} \cdot \text{L}^{-1} \text{ HCOOH} + 0.1 \text{ mol} \cdot \text{L}^{-1} \text{ H}_2\text{SO}_4$  solution at a potential scan rate of  $100 \text{ mV} \cdot \text{s}^{-1}$  at room temperature, with the currents normalized to the respective effective ECSA (Fig. 3A) and mass loading (Fig. 3B) of Pd. It can be seen that in the positive going scan, the peak potentials for HCOOH oxidation can be identified at about  $0.025 \text{ V}$  (Pd-CNPs) and  $0.10 \text{ V}$  (Pd black), respectively. The negative shift ( $\sim 75 \text{ mV}$ ) of the oxidation potential indicates an enhanced electrocatalytic activi-

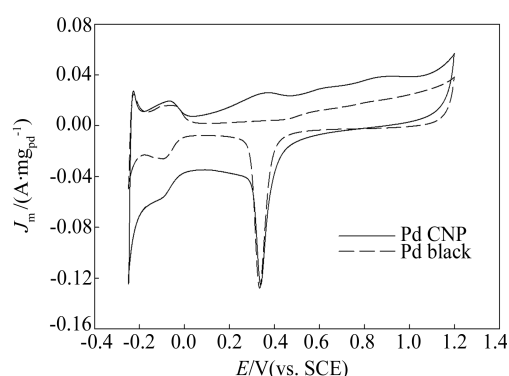


Fig. 2 Cyclic voltammograms of the Pd-CNP nanoparticles and commercial Pd black loaded onto a GC electrode in  $0.1 \text{ mol} \cdot \text{L}^{-1} \text{ H}_2\text{SO}_4$  at a potential scan rate of  $0.1 \text{ V} \cdot \text{s}^{-1}$  (the currents were normalized by the respective mass loadings of Pd).

ty of the Pd-CNP nanoparticles, an important attribute in increasing the working voltage of fuel cells. More significantly, the mass-normalized peak current density of the Pd-CNP nanoparticles is as high as  $1.15 \text{ A} \cdot \text{mg}_{\text{Pd}}^{-1}$ , which is about 2.8 times higher than that of the Pd black ( $0.40 \text{ A} \cdot \text{mg}_{\text{Pd}}^{-1}$ ). This mass activity is also highly comparable to those reported so far for state-of-the-art Pd/C (which are in the range  $1.4$  to  $2.7 \text{ A} \cdot \text{mg}^{-1}$ )<sup>[7, 24-25]</sup>, Pd nanosheets ( $1.38 \text{ A} \cdot \text{mg}^{-1}$ )<sup>[26]</sup>, and Pt-Pd alloy nanoparticles ( $1.1 \text{ A} \cdot \text{mg}^{-1}$ )<sup>[27]</sup>. Similar behaviors can be seen with the area-normalized peak current density which is  $6.22 \text{ mA} \cdot \text{cm}^{-2}$  for the Pd-CNP nanoparticles, about 2.7 times higher than that of the Pd black ( $2.29 \text{ mA} \cdot \text{cm}^{-2}$ ). The enhanced per-

formance of the Pd-CNP nanocomposite catalysts might be, at least in part, ascribed to the cauliflower-like surface morphologies that endowed the catalysts with a large effective surface area as well as the formation of abundant active sites for catalytic reactions.

The stability of the electrocatalysts under continuous operating conditions was further examined by chronoamperometric measurements. Panels C and D in Fig. 3 show the variations of the area- and mass-normalized current densities with time recorded at  $0.0 \text{ V}$  for  $600 \text{ s}$ . It can be seen that the initial activity of the Pd-CNP nanoparticles is markedly higher than that of Pd black. Yet, it decays rapidly and eventually both catalysts exhibited rather comparable electrocatalytic performance.

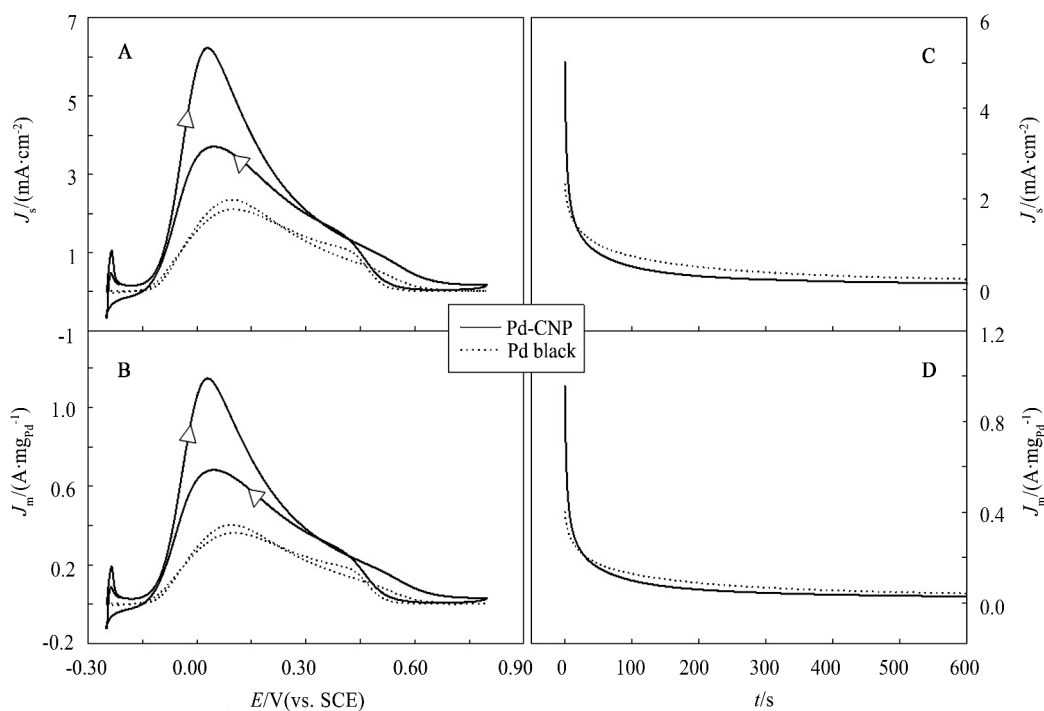


Fig. 3 Cyclic voltammograms (A, B) and current-time curves (C, D) for HCOOH oxidation at a GC electrode modified by Pd-CNP nanoparticles (solid curves) or commercial Pd black (dotted curves) in  $0.1 \text{ mol} \cdot \text{L}^{-1}$  HCOOH +  $0.1 \text{ mol} \cdot \text{L}^{-1}$  H<sub>2</sub>SO<sub>4</sub> at room temperature (Pd loading on the GC electrode was  $60 \mu\text{L}$ , while  $2.5 \mu\text{L}$  for Pd-CNP nanoparticles and Pd black, respectively, in order to obtain similar electrochemical surface areas).

Panels A and B depict the cyclic voltammograms with the currents normalized by the mass loadings of Pd and by the effective ECSA at a potential scan rate of  $100 \text{ mV} \cdot \text{s}^{-1}$ , respectively.

Panels C and D depict the current-time curves acquired at  $0.0 \text{ V}$  from  $0$  to  $600 \text{ s}$  with the currents normalized by the mass loadings of Pd and by the effective ECSA, respectively.

## 4 Conclusions

In summary, in this study we prepared Pd nanostructures supported on carbon nanoparticles (Pd-CNP) by a chemical reduction method. The resulting nanocomposite exhibited apparent electrocatalytic activity in formic acid oxidation, which exhibited a marked improvement as compared to that of commercial Pd black catalysts. This is most likely due to the cauliflower-like surface morphologies of the Pd nanostructures that exhibited enhanced accessibility of the catalyst surface and produced abundant active sites for the catalytic reactions. Further studies are desired to elucidate the electronic structures of the Pd-CNP nanocomposite catalysts.

## Acknowledgments

This work was supported, in part, by the National Science Foundation (CHE-1012256 and DMR-0804049) and by the ACS-Petroleum Research Fund (49137-ND10). J. Huang was supported, in part, by a research fellowship from the China Scholarship Council. TEM work was performed as a User Project at the National Center for Electron Microscopy, Lawrence Berkeley National Laboratory, which is supported by the US Department of Energy.

## References:

- [1] Liu H S, Song C J, Zhang L, et al. A review of anode catalysis in the direct methanol fuel cell[J]. *Journal of Power Sources*, 2006, 155(2): 95-110.
- [2] Yu X W, Pickup P G. Recent advances in direct formic acid fuel cells (DFAFC)[J]. *Journal of Power Sources*, 2008, 182(1): 124-132.
- [3] Rhee Y W, Ha S Y, Masel R I. Crossover of formic acid through Nafion<sup>®</sup> membranes [J]. *Journal of Power Sources*, 2003, 117(1/2): 35-38.
- [4] Sun S G, Clavilier J, Bewick A. The mechanism of electrocatalytic oxidation of formic acid on Pt(100) and Pt(111) in sulphuric acid solution: An emirs study[J]. *Journal of Electroanalytical Chemistry*, 1988, 240(1/2): 147-159.
- [5] Osawa M, Komatsu K, Samjeske G, et al. The role of bridge-bonded adsorbed formate in the electrocatalytic oxidation of formic acid on platinum[J]. *Angewandte Chemie-International Edition*, 2011, 50(5): 1159-1163.
- [6] Zhou W P, Lewera A, Larsen R, et al. Size effects in electronic and catalytic properties of unsupported palladium nanoparticles in electrooxidation of formic acid[J]. *Journal of Physical Chemistry B*, 2006, 110(27): 13393-13398.
- [7] Zhou W J, Lee J Y. Particle size effects in Pd-catalyzed electrooxidation of formic acid[J]. *Journal of Physical Chemistry C*, 2008, 112(10): 3789-3793.
- [8] Vidal-Iglesias F J, Solla-Gullon J, Herrero E, et al. Pd adatom decorated (100) preferentially oriented Pt nanoparticles for formic acid electrooxidation[J]. *Angewandte Chemie-International Edition*, 2010, 49(39): 6998-7001.
- [9] Meng H, Wang C, Shen P K, et al. Palladium thorn clusters as catalysts for electrooxidation of formic acid[J]. *Energy & Environmental Science*, 2011, 4(4):1522-1526.
- [10] Zhou Z Y, Kang X W, Song Y, et al. Butylphenyl-functionalized palladium nanoparticles as effective catalysts for the electrooxidation of formic acid[J]. *Chemical Communications*, 2011, 47(21): 6075-6077.
- [11] Zhou Z Y, Ren J, Kang X W, et al. Butylphenyl-functionalized Pt nanoparticles as CO-resistant electrocatalysts for formic acid oxidation[J]. *Physical Chemistry Chemical Physics*, 2012, 14(4): 1412-1417.
- [12] Zheng H T, Li Y L, Chen S X, et al. Effect of support on the activity of Pd electrocatalyst for ethanol oxidation[J]. *Journal of Power Sources*, 2006, 163(1): 371-375.
- [13] Tian L, Ghosh D, Chen W, et al. Nanosized carbon particles from natural gas soot[J]. *Chemistry of Materials*, 2009, 21(13): 2803-2809.
- [14] Tian L, Song Y, Chang X J, et al. Hydrothermally enhanced photoluminescence of carbon nanoparticles[J]. *Scripta Materialia*, 2010, 62(11): 883-886.
- [15] Song Y, Kang X W, Zuckerman N B, et al. Ferrocene-functionalized carbon nanoparticles[J]. *Nanoscale*, 2011, 3(5): 1984-1989.
- [16] Nihoul G, Abdelmoula K, Metois J J. High-resolution images of a reconstructed surface structure on (111) gold platelets—Interpretation and comparison with the-

- oretical models[J]. Ultramicroscopy, 1984, 12(4): 353-366.
- [17] Golan Y, Margulis L, Hodes G, et al. Electrodeposited quantum dots. 2. High-resolution electron microscopy of epitaxial CdSe nanocrystals on (111) gold[J]. Surface Science, 1994, 311(1/2): L633-L640.
- [18] Schlotterbeck U, Aymonier C, Thomann R, et al. Shape-selective synthesis of palladium nanoparticles stabilized by highly branched amphiphilic polymers[J]. Advanced Functional Materials, 2004, 14(10): 999-1004.
- [19] Hoshi N, Kagaya K, Hori Y. Voltammograms of the single-crystal electrodes of palladium in aqueous sulfuric acid electrolyte: Pd(S)-[n(111)×(111)] and Pd(S)-[n(100) × (111)] [J]. Journal of Electroanalytical Chemistry, 2000, 485(1): 55-60.
- [20] Duncan H, Lasia A. Separation of hydrogen adsorption and absorption on Pd thin films[J]. Electrochimica Acta, 2008, 53(23): 6845-6850.
- [21] Liang H P, Lawrence N S, Jones T G J, et al. Nanoscale tunable proton/hydrogen sensing: Evidence for surface-adsorbed hydrogen atom on architected palladium nanoparticles[J]. Journal of the American Chemical Society, 2007, 129(19): 6068-6069.
- [22] Rand D A J, Woods R. The nature of adsorbed oxygen on rhodium, palladium and gold electrodes[J]. Journal of Electroanalytical Chemistry, 1971, 31(1): 29-38.
- [23] Fang L L, Tao Q A, Li M F, et al. Determination of the real surface area of palladium electrode[J]. Chinese Journal of Chemical Physics, 2010, 23(5): 543-548.
- [24] Chen M, Wang Z B, Zhou K, et al. Synthesis of Pd/C catalyst by modified polyol process for formic acid electrooxidation[J]. Fuel Cells, 2010, 10(6): 1171-1175.
- [25] Cheng N C, Lv H F, Wang W, et al. An ambient aqueous synthesis for highly dispersed and active Pd/C catalyst for formic acid electro-oxidation [J]. Journal of Power Sources, 2010, 195(21): 7246-7249.
- [26] Huang X Q, Tang S H, Mu X L, et al. Freestanding palladium nanosheets with plasmonic and catalytic properties[J]. Nature Nanotechnology, 2011, 6(1): 28-32.
- [27] Baranova E A, Miles N, Mercier P H J, et al. Formic acid electro-oxidation on carbon supported Pd<sub>1-x</sub>Pt<sub>x</sub> (0 ≤ x ≤ 1) nanoparticles synthesized via modified polyol method[J]. Electrochimica Acta, 2010, 55(27): 8182-8188.

## 碳纳米粒子支撑的钯纳米催化剂在甲酸氧化中的电催化活性

黄 洁<sup>1,2</sup>, 周志有<sup>1</sup>, 宋 洋<sup>1</sup>, 康雄武<sup>1</sup>, 刘 珂<sup>1</sup>, 周万城<sup>2</sup>, 陈少伟<sup>1\*</sup>

(1. 加利福尼亚大学化学与生物化学系, 美国 圣克鲁兹 95064;

2. 西北工业大学凝固技术国家重点实验室, 陕西 西安 710072)

**摘要:** 采用化学还原法制备了碳纳米粒子支撑的钯纳米结构(Pd-CNP). 透射电镜表征显示在 Pd-CNP 纳米复合物中, 金属 Pd 呈菜花状结构, 粒径约 20 ~ 30 nm. 它们由许多更小的 Pd 纳米粒子(3 ~ 8 nm)组成. 电化学研究表明, Pd-CNP 的电化学活性面积比商业 Pd 黑低 40%, 可能原因是部分 Pd 表面被一层碳纳米粒子覆盖, 但其对甲酸氧化却表现出更好的电催化活性, 质量比活性和面积比活性都比 Pd 黑高几倍. 催化活性增强的原因可能是碳纳米粒子支撑的 Pd 纳米结构具有特殊的层次化结构, 可以形成更多的活性位, 以及表面位更利于反应进行.

**关键词:** 钯纳米结构; 碳纳米粒子; 甲酸电氧化; 燃料电池